The Journal of Supercritical Fluids 177 (2021) 105331

Contents lists available at ScienceDirect

The Journal of Supercritical Fluids

journal homepage: www.elsevier.com/locate/supflu

Cold neutron transmission for the in-situ analysis of the gas diffusion in polymers

Judith Martín-de León [a,b,*], Paula Cimavilla-Román [a], Victoria Bernardo [a,b], Eusebio Solórzano [a], Nikolai Kardjilov [a,c], Miguel A. Rodríguez-Pérez [a]

[a] Cellular Materials Laboratory (CellMat), Universidad de Valladolid, 47011, Spain
[b] CellMat Technologis S.L., Paseo de Belen 9A, 47011 Valladolid, Spain
[c] Institute of Applied Materials, Helmholtz-Zentrum Berlin, Berlin, Germany

HIGHLIGHTS

- In-situ visualization of gas diffusion process in polymers.
- Neutron radiography and tomography of gas diffusion in polymers.
- In situ dimensions evolution of polymers under gas pressure.
- In situ solubility and diffusivity evolution of polymers under gas pressure.

GRAPHICAL ABSTRACT

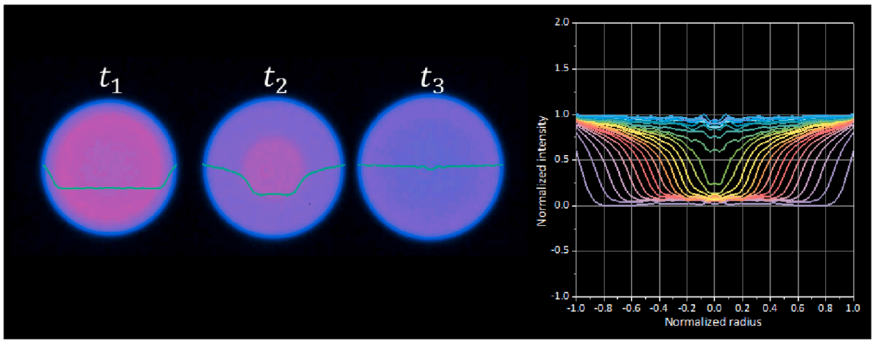

ARTICLE INFO

Keywords:
Diffusion mechanisms
Gas dissolution
Swelling
CO_2 absorption

ABSTRACT

A novel set-up for monitoring the gas diffusion process in polymers has been developed. This set-up is based on performing neutron radiography and tomography of polymeric materials under high pressures of gas. Information about the absorption kinetics of supercritical CO_2 was obtained. Additionally, solubility, diffusivity, and macroscopic changes in the dimensions of the samples can be in-situ obtained through the developed measurement technique. This novel approach can be very helpful to analyze the diffusion kinetics in a wide range of polymers.

1. Introduction

Gas diffusion is a universal phenomenon that happens all over daily life. From minor issues such as the gas losses in soft-drinks to the breathing process without which humans could not live. The physics behind the diffusion phenomena is essential for the understanding of all these processes.

Besides in nature, gas diffusion has become an essential tool in some industries. Particularly, methods based on diffusion of supercritical carbon dioxide (sc-CO_2) into polymers are widely used in sectors such as

* Corresponding author at: Cellular Materials Laboratory (CellMat), Universidad de Valladolid, 47011, Spain.
E-mail address: jmadeleon@fmc.uva.es (J. Martín-de León).

https://doi.org/10.1016/j.supflu.2021.105331
Received 9 April 2021; Received in revised form 12 June 2021; Accepted 27 June 2021
Available online 1 July 2021

automotive, building, food packaging, or pharmaceutical, among others. For example, pharmacology takes advantage of sc-CO_2 by dissolving different drugs into final porous polymeric matrixes employing a diffusion process, usually called solvent impregnation method [1–4].

Additionally to pharmacological applications sc-CO_2 is a key factor for some processes implying polymer processing such as impregnation, extraction or modification of polymeric materials [5]. Gas diffusion is also a crucial tool to produce microcellular polymers that are industrially manufactured for a wide range of applications. Several companies distribute microcellular polymer products in the form of films, sheets, or blow molding parts that meet the needs of several applications such as food packaging, bags, ducts, or industrial pipes [6–8]. Expanded polypropylene (EPP) parts are also produced via a CO_2 diffusion-based method [9,10]. Gaming pieces, furniture parts, or lightweight construction components are made of EPP, but especially the automotive sector cannot be understood nowadays without these materials; car bumpers, battery covers, roof pillars, or seat bracing are developed from this microcellular polymer and distributed by companies all around the world. The thermal insulation sector especially takes advantage of microcellular products. Additionally, gas diffusivity plays a key role in this sector also to produce vacuum insulated panels (VIP), or the study of gas losses in thermal insulating materials (such as the diffusivity of pentane out of polyurethane foams)[11–13]. Still, in the cellular polymer's framework, the gas diffusion process is also used to produce new and promising materials such as nanocellular polymers [14,15].

The control of the diffusion process parameters (such as used pressure, temperature, or depressurization rate) as well as the study of the interaction between the gas and the polymer are critical for the characteristics of the final product in all the mentioned applications. When considering microcellular polymers, parameters such as the final density or the final cell size of the cellular material are strongly affected by the diffusion conditions [16–18]. Referring to the impregnation methods, the amount of the dissolved drug inside the polymer depends on the saturation pressure, temperature, and time [19–21]. Another topic in which diffusion phenomena is critical is the development of multilayer thin films for food packaging applications. Extending the lifetime of food strongly depends on proper control of gas diffusion (oxygen, nitrogen, carbon dioxide, and water vapor) through these types of thin films [22].

On the one hand, the interaction between sc-CO_2 and polymers has been studied through spectroscopy methods, such as Raman or IR spectroscopy [5,23,24]. On the other hand, to understand and control the diffusion process, it is key to develop experimental methods that could in-situ measure the diffusion of the gas phase in the polymeric matrix. A commonly used technique is the magnetic suspension balance, presenting this method multiple drawbacks. On the one hand, during the diffusion experiment, the material suffers a volume change (swelling) necessary to consider in the mass measurement. Some authors already solved this limitation by implementing a visual complementary method accounting for the swelling effect [26]. On the other hand, this technique only allows obtaining a global measurements of parameters such as solubility and diffusivity, being not possible to have spatial resolution [25]. However, it is not easy to develop improved alternatives based on in-situ measurements. Experiments to characterize the diffusion of a gas in a polymeric material need to be carried out inside a pressure vessel suitable for achieving the high-pressure atmosphere required. This constitutes a major drawback for the analysis of these processes, firstly, because pressure vessels are typically made of heavy elements such as steel what makes difficult the use of common non-destructive imaging systems, such as X-rays due to the high attenuation when passing through these heavy elements and the low contrast between the gas and the background [27]. Secondly, when working with gas-solid systems, it is impossible to freeze the process so spatial resolution can only be obtained through in-situ techniques. Taking these ideas in mind, it is possible to guess that cold neutrons offer a perfect alternative due to their weak interaction with matter what makes them very penetrating, being possible to visualize what is happening inside a metal cell. Additionally, the interaction of neutrons with chemical elements varies randomly across the periodic table, leading to high contrast [28].

In this paper, a pioneering set-up to perform in situ radiography and tomography experiments of the gas dissolution process in solid materials under high-pressure atmospheres is presented and used to characterize the behavior of two different polymers, polystyrene (PS) and polymethylmethacrylate (PMMA), under CO_2. This system allows monitoring the whole process thanks to the use of cold neutrons, gathering information about the sc-CO_2 absorption kinetics. Furthermore, it allows obtaining information about the morphological changes in 3D in the saturated system. Thus, qualitative and quantitative information regarding the swelling, the solubility and the diffusivity have been obtained for two different polymeric systems studied at different diffusion conditions.

2. Theoretical background

Fick's second law describes the diffusion of the gas inside a polymer, according to Eq. 1,

$$\frac{\partial C}{\partial t} = \nabla(D\vec{\nabla}C) \tag{1}$$

where C is the concentration of gas and D is the diffusion coefficient [29]. Different saturation conditions induce different behaviors in the gas/polymer system; for example, higher pressures lead to higher solubilities and diffusivities, while higher temperatures imply lower solubilities but also an increase of the velocity of diffusion of the gas [30–32]. Furthermore, polymers suffer an increase in their volume when gas diffuses inside them, an effect known as swelling. Swelling is dependent on the saturation conditions as well as on the polymer and gas nature [33,34].

Other essential concept in this work is neutron transmittance. The attenuation of a neutron beam passing through a polymer is due to coherent and incoherent scattering and absorption of neutrons by the nuclei conforming the polymer chains (carbon, oxygen, and hydrogen). The transmission of neutrons T, through a polymer can be described by Beer's law [35–37]:

$$T = I/I_0 \quad = e^{-\mu \cdot l} \tag{2}$$

where I is the intensity through the sample, I_0 is the incident intensity, μ is the attenuation coefficient and l is the radius of the sample (for cylindrical samples). The introduction of a new phase inside the polymer, such as CO_2, leads to a decrease of the total transmission and therefore an increase in the attenuation coefficient, due to the scattering and absorption of neutrons by the gas, being now the attenuation coefficient a combination of the contributions given by the polymer and the dissolved gas [38]. Therefore, the sorption process of gas inside the polymer should result in a change of the transmittance and the attenuation coefficient that can be related with the parameters defining the diffusion process, such as solubility, i.e., the amount of absorbed gas, or diffusivity, the rate at which gas penetrates the polymer.

3. Experimental section

3.1. Materials

Commercial cylindrical polymeric samples with 4 mm in diameter of polystyrene (PS) and polymethylmethacrylate (PMMA) have been used in the diffusion experiments.

PMMA V825T has been kindly supplied by ALTUGLAS® International (Colombes, France). This polymer presents a density of 1.19 g/cm^3 with a glass transition temperature of 114 °C (measured by DSC) and a melt flow index of 1.92 g/10 min (measured at 200 °C with 5 kg of weight).

EDISTIR® N 2380 by Versalis Eni Group has a density of 1.05 g/cm^3,

accompanied with a glass transition temperature of 104 °C and a melt flow index of 2 g/10 min (measured at 200 °C with 5 kg of weight).

3.2. Set up description

Experiments were performed at the neutron imaging instrument at the BER-2 research reactor of the Helmholtz-Zentrum Berlin, CONRAD 2 [39,40]. This curved guide of the reactor filters the high-energy neutrons and gammas from the core of the reactor achieving a neutron spectrum at the end of the guide that presents a maximum of 2.5 Å, that is, cold neutrons, that allow performing high-resolution tomography. For this study, a pinhole diameter of 2 cm was used reflected in collimating ratios L/D of 500. A high-resolution detector system with a pixel size of 13.5 μm yielded a spatial resolution of 23.36 μm with a field of view of 30 × 30 cm^2. The detector exposure time was fixed in 1 s, and each tomography experiment consisted of a set of 600 projections covering an angular interval of 360°. One tomography was completed every 10 min resulting in total measuring times from 8 to 14 h.

The set-up to perform the diffusion experiments is shown in Fig. 1. It was placed on the rotation table at the end of the line with the neutron beam pointing at the pressure pipe where the sample of interest is placed. The novelty of this apparatus relies on the possibility of performing high-resolution tomographies of a rotating sample under high pressures of gas. On the one hand, credit is due to the small eccentricity achieved with the rotation system, and on the other hand, to the whole self-constructed set-up that allows reaching high pressures while the sample is rotating. As shown in Fig. 1, the rotation system attached to the rotation table comprises a magnetic stirrer (2) (Mini 100 from PREMEX GmbH) connected to a self-constructed sample holder (5), through a connector ensuring the non-eccentric rotation (3). The sample holder is provided with some screws guaranteeing the immobility of the sample during the whole experiment. This sample holder is placed inside the aluminum pipe acting as pressure vessel (4), that is connected with a CO_2 bottle and a gas booster, allowing the system to work up to pressures of 20 MPa. Additionally, a heating blanket (6) (12 V/12 W) and a temperature controller make it possible to reach temperatures up to 80 °C.

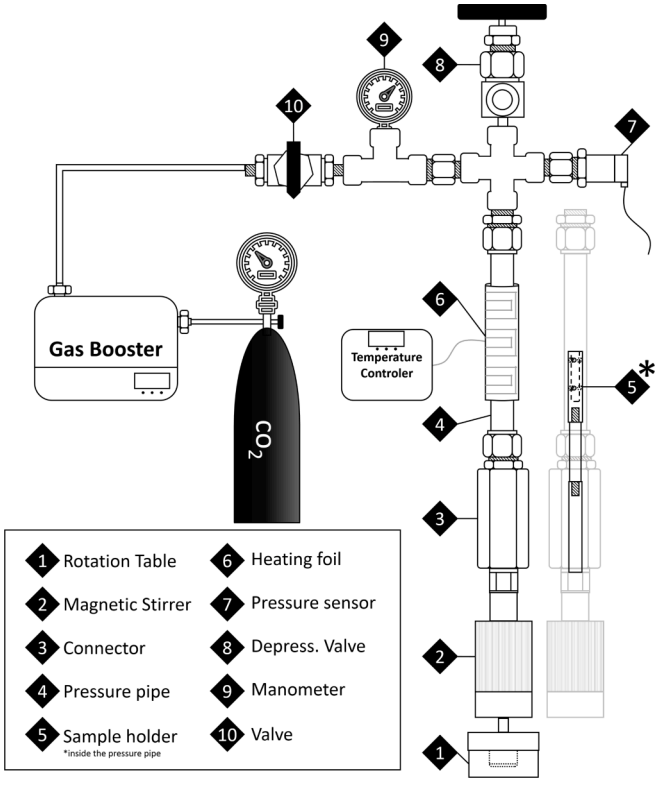

Fig. 1. Scheme of the used set-up for performing the in-situ diffusion experiments.

The whole installation allows performing experiments with a wide range of saturation parameters (gas pressure and temperature). In this work, diffusion experiments were performed under pressures ranging from 10 to 20 MPa, temperatures of 40 °C and 60 °C and times of 5–11 h and the results have been analyzed in different ways that are explained in the next paragraphs.

3.3. Ex situ calibration

An ex-situ calibration was performed to verify the proposed method. The experiment was carried out in the set-up described as follows. The system comprises a pressure vessel (model PARR 4681) provided by Parr Instrument Company (Moline, IL, USA) that allows working at 41 MPa combined with 350 °C of temperature. In order to provide the vessel with the required pressure, a pressure pump (model SFT-10) supplied by Supercritical Fluid Technologies Inc. (Newark, DE, USA) is used. On the other hand, the control of the temperature is accomplished through a thermal jacket of 1200 W connected to a temperature controller (CAL 3000). Five saturation experiments were performed in this set-up with different saturation times from 30 min to 14 h. After each experiment, the amount of gas uptake was determined by doing an extrapolation of the mass vs time curve at zero time, with a desorption time (time from the release of the pressure to the first mass measure) of 1.5 min in all the experiments [41].

3.4. Radiography

The proposed set-up, together with the acquisition method and data processing, allows to in-situ measure for the first time in 3D the changes taking place in a polymer subjected to an sc-CO_2 diffusion process. To obtain the maximum amount of information, the acquired tomographies have been analyzed in two different ways. Firstly, the projection images, this is, the raw data obtained, have been investigated, obtaining images like that shown in Fig. 2. These projection images, initially obtained as a 16-bit grayscale map, were later treated to produce color images improving this way the visual dynamic range. The transmission through the cylinder has been calculated by considering the intensity I as the average gray value of a region of interest inside the sample and the initial intensity I_0 as the mean gray value of the region of interest outside of the sample but inside the pipe vessel (Fig. 2). Five images per tomography at different time instants for every experiment have been analyzed by following the same procedure, calculating the temporal evolution of transmissivity of the gas-polymer system.

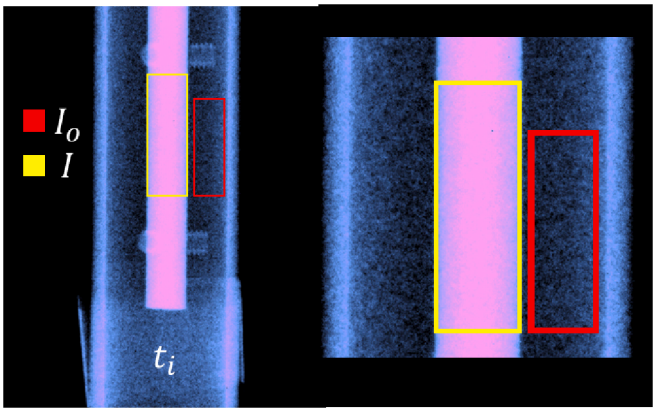

Fig. 2. Image for the radiography analysis of the samples. Two examples of the region of interest considered in determining the transmittance are showed.

3.5. Tomography

The second approach to analyze the data is to use the tomography data in 3D. Tomography experiments were reconstructed using the filtered back-projection algorithm implemented in the commercial software tool Octopus [42]. The reconstruction process yields cross-section images of the material in which the pixels take values reflecting the corresponding neutron attenuation coefficients [43]. One direct application of these measurements is determining the volume increase of the samples (swelling).

Due to polymers are strong absorbers of cold neutrons, the reconstructed cross-section of the material shows a central region darker than the edges. The beam hardening effect causes this lack of linearity in the line profile through the sample. Therefore prior to the tomography reconstruction, it is necessary to apply a beam hardening correction algorithm implemented in Octopus. Afterward, a noise filter is used, and the position of the center of rotation is calculated as well as the offset angle of the same axis of rotation [44]. Afterward, the alignment of the vertical slices is carried out to correct the horizontal displacement of the center of rotation along with the sample's height. Each tomography reconstruction consists of a set of 1000 cross-section images that are later averaged to enhance any absorption changes through the sample. This procedure results in a single cross-section image per tomography where each voxel depicts the average attenuation coefficient of the sample during the experiment time. By following the same procedure for each tomography, the temporal evolution of the radial profile of the attenuation coefficient can be obtained (Fig. 3).

The in-depth analysis described has led to the visualization of the whole diffusion process and quantifying the parameters defining it.

4. Results

4.1. Swelling

Firstly, morphological changes in the polymer due to gas diffusion were quantified. As Fig. 3 illustrates, gas absorption involves an increase in the total diameter of the sample (swelling). By knowing the initial radius of the cylinder, it is possible to quantify the percentage of volume increase of the sample during the whole diffusion experiment. Obtained results are shown in Fig. 4 and Table 1.

Swelling values for PMMA are high in the conditions used in these experiments (between 25% and 30% volume increment). This is due to the high solubility of CO_2 in this polymer which is known to be a CO_2-philic polymer [45].

Changes between saturation conditions and between polymers are detected. Thus, when maintaining the saturation temperature in 40 °C, PMMA shows an increase of the swelling from 24.1% to 30.47% with a saturation pressure increment from 10 to 20 MPa. The change in the volume as a consequence of gas diffusion is closely related to the amount of gas uptake (from 20.06% to 23.17%). A higher saturation pressure leading to a higher amount of gas uptake results in a higher increase in the volume of the material.

This volume increment is also affected by the saturation temperature, as it can be seen for PMMA samples. An increase in saturation temperature from 40 to 60 °C leads to higher mobility of polymeric chains, leading to a slightly higher swelling for similar solubilities.

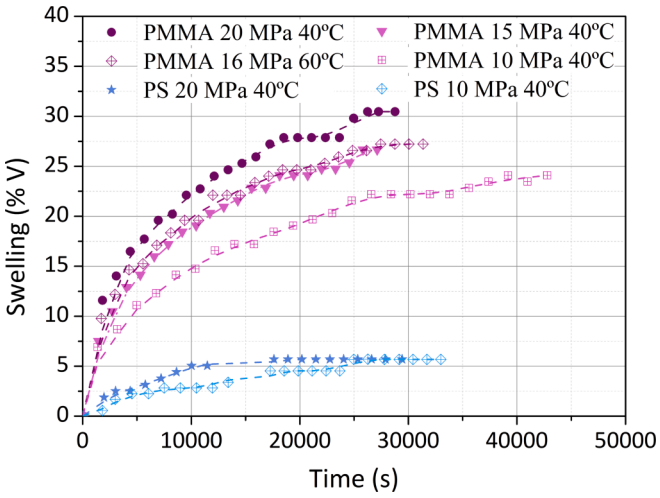

Fig. 4. Time evolution of swelling for the different experiments.

Polystyrene present much more smaller values of swelling, less than 5% for the experiments performed at 40 °C and with saturation pressures of 10 and 20 MPa, which is related with the much lower solubility of CO_2 in this polymer, around 9 wt% in comparison with values higher than 25 wt% for PMMA.

The final obtained values agree with those shown in the bibliography. For PMMA, Nikitin et al. reported swelling values between 22% and 29% for 38 °C of saturation temperature and pressures between 9 and 20 MPa [46]. While Rajendran et al. presented values between 20% and 23% for 50 °C of saturation temperature and pressures from 12 to 19 MPa [47,48]. Values in the literature for PS show swelling values around 20% for pressures smaller than 20 MPa and low temperatures [33]. It can be concluded that our method has enough resolution to detect morphological changes during the gas diffusion process.

5. Radiography

As previously commented the gas absorption leads to a change in the neutron transmittance through the cylinder that can be calculated with radioscopy analysis. On the other hand, as explained before, the swelling is directly related to gas diffusion inside the polymer. To obtain the evolution of the transmittance with time, it is necessary to process the radioscopy data together with the swelling measurements previously obtained. The radius (l) of the sample is increasing during the experiment, so to obtain comparable transmittance values along time, a factor considering this radius increase was introduced normalizing this way all the transmittance values to the initial diameter of the sample (l_0). Thus, the normalized transmittance, T_0, can be calculated from the transmittance T measured in any time through Eq. 3 directly derived from Eq. 2.

$$T_0 = T^{l_0/l} \tag{3}$$

where l_0 is the initial radius and l is the radius at a given time.

After the radiography analysis, graphs as that shown in Fig. 5a were obtained. It can be seen how the method allows detecting the decrease of

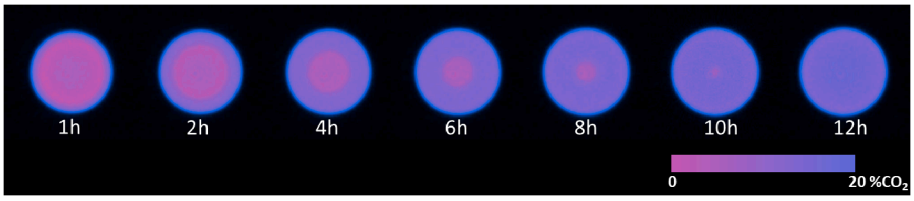

Fig. 3. Time evolution of the cross-section images obtained through tomography analysis for the sample saturated at 10 MPa and 40 °C.

Table 1
Data the experiments. Saturation pressures, saturation time, solubility, diffusivity and swelling.

Material	Saturation pressure (MPa)	Saturation temp. (°C)	Saturation time (h)	Solubility (wt%)	Diffusivity (cm^2/s)	Swelling (vol%)
PMMA	10	40	10.6	20.06	$1.1{\cdot}10^{-6}$	24.10
PMMA	15	40	7.1	21.86	$2.0{\cdot}10^{-6}$	26.66
PMMA	20	40	4.7	23.17	$4.0{\cdot}10^{-6}$	30.47
PMMA	16	60	4.7	21.23	$3.9{\cdot}10^{-6}$	27.22
PS	10	40	11.1	8.93	$1.0{\cdot}10^{-6}$	4.29
PS	20	40	7.1	9.24	$1.8{\cdot}10^{-6}$	4.85

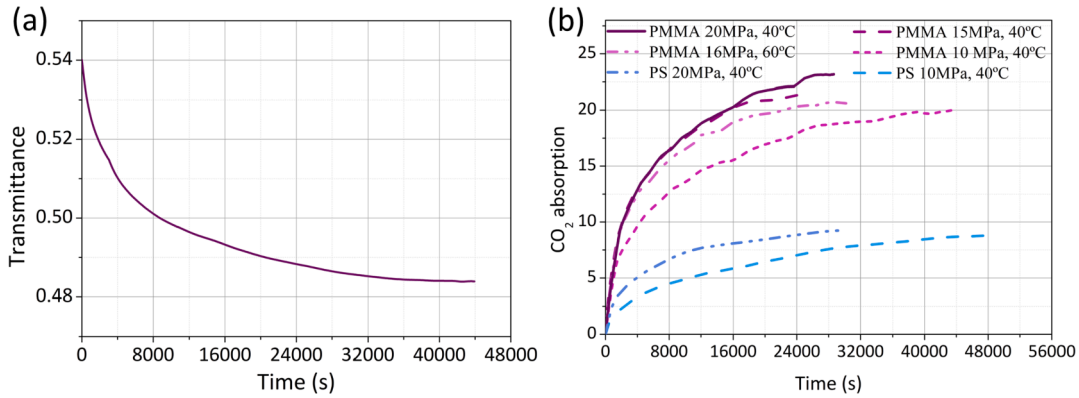

Fig. 5. a) Example of the transmittance evolution with time for the sample of PMMA saturated at 10 MPa and 40 °C. b) Solubility values obtained during the whole experiment for all the tests carried out.

the transmittance due to gas diffusion; the introduction of the second phase (the gas) is leading to a higher neutron absorption reflected in the measured transmittance values. This significant change gives us the chance to quantify the total amount of gas absorbed, that is, the solubility in the sample, in each instant of time. The initial transmittance (T_0) is related to the initial amount of gas C_0, it means zero, and the final value of transmittance, T_f is linked with the final amount of CO_2 uptake C_f. This final amount of gas C_f is calculated as the percentage of weight increment of the gas-polymer mixture. This weight was experimentally measured by means of weighting the sample immediately after the whole experiment in a precision balance and extrapolating the data to zero desorption time [49]. Desorption time was fixed to be 2.5 min in all the performed experiments. Then, the amount of gas inside the sample for each instant of time (C_i) can be obtained using Eq. 4:

$$C_i = C_f \cdot \frac{T_i - T_0}{T_f - T_0} \tag{4}$$

Through this equation CO_2 absorption curves can be obtained (Fig. 5b).

To verify the performed calibration, an ex-situ experiment was carried out with the same PMMA by saturating this material at 15 MPa and 60 °C of saturation pressure and temperature, respectively as explained in the experimental section.

The obtained experimental points were compared with the obtained curve by using neutrons transmission. As it can be seen in Fig. 6a, an accurate fitting between the two set of experimental data were obtained. Desorption time is smaller in this ex-situ calibration as previously commented, however values in both methods fit meaning that the approximation to zero desorption time is valid in this range of times.

The solubility data measured in the paper are clearly related to the

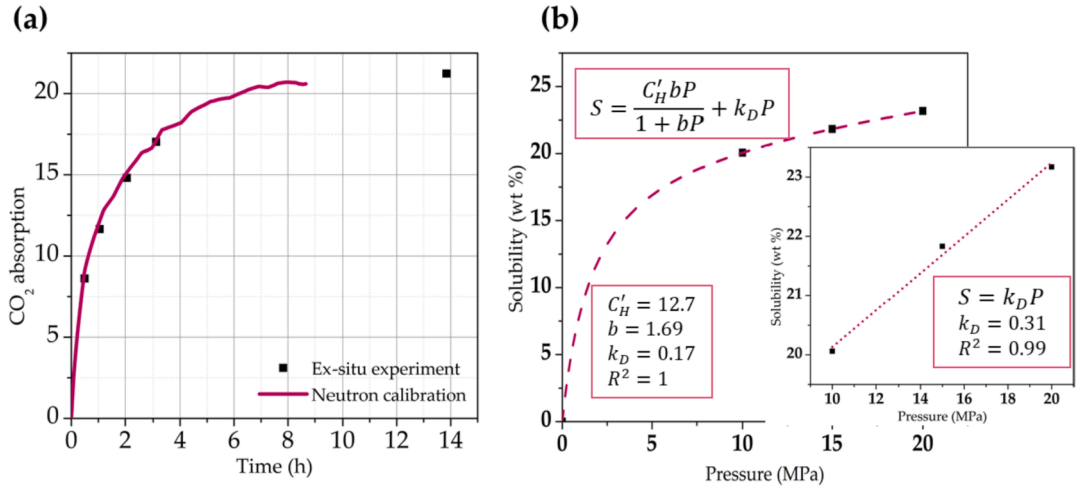

Fig. 6. a) Comparison between ex-situ sorption experiments with the in-situ solubility curve obtained with the method proposed in the paper. b) Linear relationship between solubility and pressure in the studied range for PMMA.

used saturation conditions. As it can be seen in Fig. 5 and Table 1 when fixing the saturation temperature at 40 °C, an increase in the saturation pressure from 10 MPa to 20 MPa results in a raise of solubility for PMMA from 20 wt% to 23 wt%. As well as for PS from 8.93 wt% to 9.24 wt%.

Different models give the dependence of solubility with pressure. The simplest one is Henry model that relates solubility linearly with pressure through the Henry constant k_D. Although this relationship fits for a wide range of process parameters and polymers, non-linear models are sometimes needed such as the Langmuir or Dual models [29,50,51].

Fig. 6b shows the fitting for the obtained data in this work for PMMA. Assuming that no pressure is associated to zero solubility, data points adjust to the dual model, by using $C_H^{'} = 21.5, b = 0.59$ and $k_D = 0.17$. In addition, limiting the analysis to the range of used pressures the measured data fit properly with Henry equation by using a value of $k_D = 0.3$.

Conversely, when maintaining the saturation pressure at 15 MPa, the increase in the saturation temperature from 40 °C to 60 °C is translated in a solubility reduction (Table 1). Attending to Eq. 5, the dependence of the solubility with temperature is given by Arrhenius equation [52]:

$$S = S_0 \exp\left(-\frac{\Delta H_s}{RT_{sat}}\right) \tag{5}$$

where S_0 is the preexponential factor, ΔH_s is the heat of sorption, R is the gas constant, and T_{sat} is the saturation temperature. Taking into account that the heat of sorption is negative for CO_2/PMMA system [41], an increase in the saturation temperature results in a decrease in the solubility as it is measured by approach proposed in this paper.

Although solubility would depend on the characteristics of the used PMMA, data in the literature for saturation temperatures between 40 and 60 °C, range between 20 and 25 wt% that are similar to the values measured a in this work [46,53].

Regarding PS, solubility values are much smaller than for PMMA, fact also supported by the literature [54], although the sorption dynamics is slower for 10 MPa, the final amount of gas uptake is similar, 9.2 wt% for 10 MPa and 9.6 wt% for 20 MPa. This fact has been reported in different papers and for various saturation temperatures were it was demonstrated that solubility on PS firstly increases with the increase of pressure up to pressure were the solubility almost stabilizes [30,54,55]. The differences between the solubility of PMMA and PS at the same saturation conditions are high. PMMA absorbs at least 10% more gas than PS.

6. Tomography

The reconstructed tomography slices analysis allows obtaining the temporal evolution of the diffusion profile of gas inside the polymer and determining the diffusivity and the saturation time. As it was shown in Fig. 3, the cross-section of the sample shows, on the one hand, radial changes in the attenuation coefficient, and on the other hand, the temporal evolution of this radial profile. These differences are due to the gas penetrating the sample; the lighter shades signal the lack of gas in the solid, while the darkest ones mark this second phase inside the polymer. It is clear how the gas radially advances from the surface of the sample to the center up to reach the full saturation when the tones inside the cylinder are homogeneous.

The radial and temporal evolutions can be quantified by merely representing the radial profile of the normalized attenuation coefficient for each tomography. Fig. 7a shows an example of these curves PMMA at MPa and 40 °C. This normalized radial profile represents the Fick law's solution for diffusing a gas inside a cylinder with a diffusion coefficient dependent on the pressure [56]. Therefore, it is possible to experimentally determine the concentration distribution of gas inside the cylinder and to in-situ follow the evolution of this profile, thanks to the method developed in this work.

The evolution of the concentration profile is related to the velocity of penetration of the gas inside of the polymer.

So as to calculate diffusivity from the normalized attenuation coefficient profiles showed in Fig. 7a. it was assumed that the time of diffusion is given by the following equation [56]:

$$t \approx \frac{r^2}{2D} \tag{6}$$

The marked peak in Fig. 7a. shows the penetration depth of the gas inside the polymer for each time. By following the evolution of this peak position as a function of time, the diffusivity can be calculated as shown in Fig. 7b. Additionally, when the gas reaches the center of the cylinder it can be affirmed that the material is saturated, being this instant selected as the saturation time.

Experiments were analyzed following the described method. Fig. 8 shows how saturation conditions affect both diffusivity and saturation time for PMMA.

The dependence of the diffusion coefficient with pressure in the range under study is given by the following equation [56]:

$$D = a + bP + cP^2 \tag{7}$$

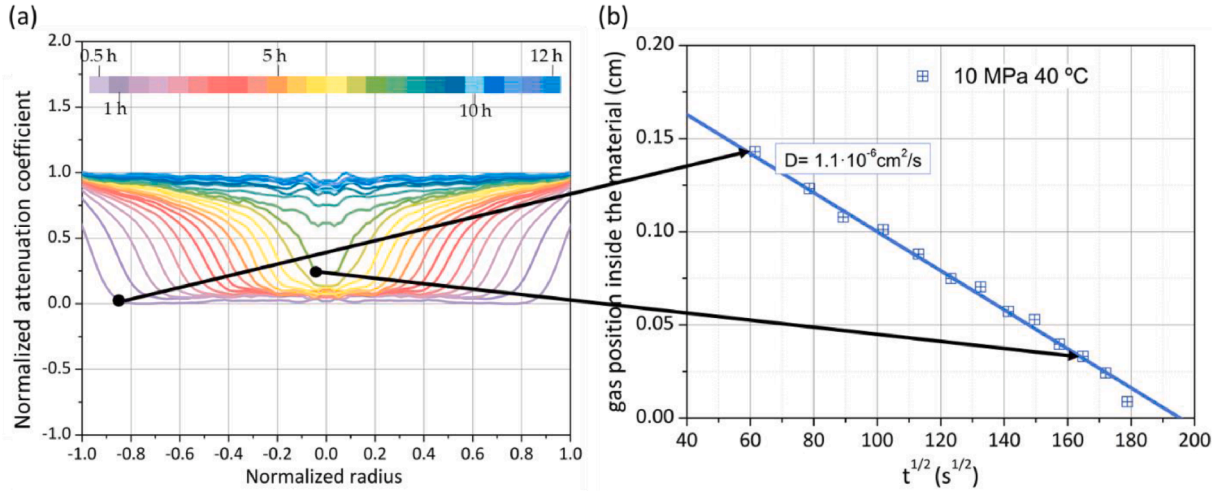

Fig. 7. a) Time evolution of the neutron intensity along the radius of the sample of PMMA saturated at 10 MPa and 40 °C. b) Example of the procedure followed to obtain the gas position inside the material as a function of the square root of time from the profiles representing the normalized attenuation coefficient as a function of the normalized radius.

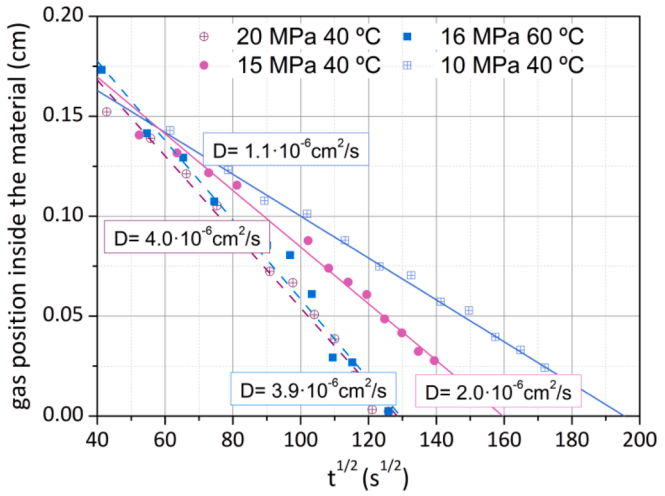

Fig. 8. Gas position inside the cylinder as a function of the square root of time to determine diffusivity and saturation time for the PMMA samples.

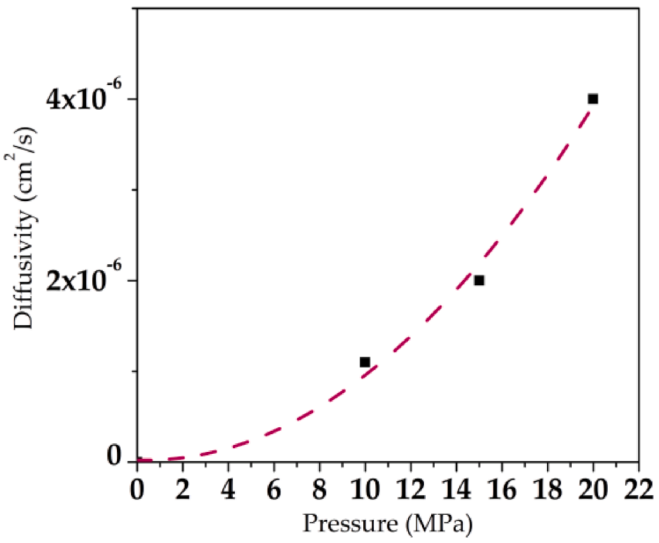

Fig. 9. Diffusivity as a function of saturation pressure, adjusted with Eq. 7.

Fig. 9 shows the data obtained in this work fitted with Eq. 7, with constant values of $a = 1.0{\cdot}10^{-8}; b = 8.4{\cdot}10^{-9}; c = 2.4{\cdot}10^{-8}$. It is clear that an increase in the pressure results in a faster absorption diffusivity (diffusivity during the absorption experiment following Fick's laws), translating in smaller saturation times (Table 1).

One mechanism that could be playing a role in the pressure dependence of diffusivity is the following one: When the gas diffuses in and starts saturating the polymer matrix, it is well known that T_g is being reduced. This reduction of T_g is particularly strong for PMMA. The reduction of the T_g favors mobility of the polymer matrix and due to this an increase in diffusivity is expected. Therefore, two different aspects may explain the strong dependence of diffusivity with pressure. In the one hand, the direct effect of increasing pressure that increases the driving force for diffusion and the indirect effect of saturating a polymer with a large dependence of T_g with the gas absorbed.

Conversely, the dependence with the temperature is given by an Arrhenius type equation [41].

$$D = D_0 \exp\left(-\frac{\Delta H_D}{RT}\right) \tag{8}$$

where D_0 is the pre-exponential factor and ΔH_D is the activation energy for the diffusion process. Although some exceptions have been reported [41], activation energy is usually positive for gas/polymer systems, so an increase in the temperature leads to higher sorption diffusivities.

That is the case in this work (Table 1), where an increase of the temperature from 40 °C to 60 °C doubles the diffusivity. The change is, in fact, equivalent to increase the pressure from 15 to 20 MPa.

Obtained data fit well with those previously reported. PMMAs with different molecular weights present sorption diffusivities ranging 10^{-6}–10^{-7} cm^2/s [46,53].

7. Conclusions

To sum up, the developed set up and the followed analysis make it possible to in-situ follow the diffusion process of a gas inside a polymer, leading to both qualitative and quantitative results. Thus, structural changes such as swelling can be followed and measured, and the evolution of the amount of absorbed gas during the whole experiment, while the concentration profile or the diffusivity and saturation time can be determined with a straightforward approach.

This method would be beneficial for the understanding of diffusion phenomena involving gas and polymeric materials. Thus, morphological changes in samples, could be controlled, and process times could be accurately adjusted. Ultimately, the developed method allows visualizing and in-situ measuring all the physical process of the diffusion phenomenon, that up to now were hidden, being possible to obtain key parameters to understand and finely control the diffusion process in polymers. This set-up can be used to obtain important novel information of applicability is various sectors of polymer science and technology such as pharmacology, cellular polymers and multi layered thin films.

Declaration of Competing Interest

The authors declare that they have no known competing financial interests or personal relationships that could have appeared to influence the work reported in this paper.

Acknowledgments

Financial assistance from the Junta of Castile and Leon (VA202P20) and Spanish Ministry of Science, Innovation, and Universities (RTI2018-098749-B-I00 and RTI2018-097367-A-I00 and PTQ2019-010560 (Victoria Bernardo-García)) and the "Ente Público Regional de la Energía de Castilla y León" (EREN) are gratefully acknowledged. Financial support from the Junta de Castilla y Leon predoctoral grant of P. Cimavilla-Román, co-financed by the European Social Fund, is also acknowledged.

References

[1] P. Marizza, L. Pontoni, T. Rindzevicius, J.F. Alopaeus, K. Su, J.A. Zeitler, S. S. Keller, I. Kikic, M. Moneghini, N. De Zordi, D. Solinas, A. Cortesi, A. Boisen, Supercritical impregnation of polymer matrices spatially confined in microcontainers for oral drug delivery: effect of temperature, pressure and time, J. Supercrit. Fluids 107 (2016) 145–152, https://doi.org/10.1016/j.supflu.2015.08.023.

[2] A. Nieto, F. Balas, M. Colilla, M. Manzano, M. Vallet-Regí, Functionalization degree of SBA-15 as key factor to modulate sodium alendronate dosage, Microporous Mesoporous Mater. 116 (2008) 4–13, https://doi.org/10.1016/J.MICROMESO.2008.03.025.

[3] L. Gao, J. Sun, Y. Li, Functionalized bimodal mesoporous silicas as carriers for controlled aspirin delivery, J. Solid State Chem. 184 (2011) 1909–1914, https://doi.org/10.1016/J.JSSC.2011.05.052.

[4] A. Szegedi, M. Popova, I. Goshev, J. Mihály, Effect of amine functionalization of spherical MCM-41 and SBA-15 on controlled drug release, J. Solid State Chem. 184 (2011) 1201–1207, https://doi.org/10.1016/J.JSSC.2011.03.005.

[5] O.S. Fleming, S.G. Kazarian, Polymer processing with supercritical fluids. Supercritical Carbon Dioxide: in Polymer Reaction Engineering, 2006, pp. 205–238, https://doi.org/10.1002/3527606726.ch10.

[6] H. Wu, E. Wintermantel, H.J. Haugen, The effects of mold design on the pore morphology of polymers produced with mucell technology, J. Cell. Plast. 46 (2010) 519–530, https://doi.org/10.1177/0021955×10376454.

[7] L.J. Hyde, L.A. Kishbaugh, The MuCell ® injection molding process: a strategic cost savings technology for electronic connectors, in: Proc. Int. Inst. Connect.

Interconnect. Technol. Inc. Annu. Symp. (2003). http://citeseerx.ist.psu.edu/viewdoc/download?doi=10.1.1.202.2075&rep=rep1&type=pdf.
[8] D. Milan, D. Peal, (12) Patent Application Publication (10) Pub. No.: US 2002/0187020 A1, 1 (2013). https://doi.org/10.1016/j.(73).
[9] M. Carley, S.R. Shoper, Vehicle bumper energy absorber system and method, 2012. https://doi.org/10.1037/t24245-000.
[10] E. Tang, S.K. Wa Leung, Molding method for expandable polypropylene, 2012. https://doi.org/10.1037/t24245-000.
[11] C.G. Yang, Y.J. Li, X. Gao, L. Xu, A review of vacuum degradation research and the experimental outgassing research of the core material – Pu foam on vacuum insulation panels, Phys. Procedia 32 (2012) 239–244, https://doi.org/10.1016/j.phpro.2012.03.549.
[12] Z. Tang, M.M. Maroto-Valer, J.M. Andrésen, J.W. Miller, M.L. Listemann, P. L. McDaniel, D.K. Morita, W.R. Furlan, Thermal degradation behavior of rigid polyurethane foams prepared with different fire retardant concentrations and blowing agents, Polymer 43 (2002) 6471–6479, https://doi.org/10.1016/S0032-3861(02)00602-X.
[13] J. Fricke, U. Heinemann, H.P. Ebert, Vacuum insulation panels – from research to market, Vacuum 82 (2008) 680–690, https://doi.org/10.1016/j.vacuum.2007.10.014.
[14] B. Notario, A. Ballesteros, J. Pinto, M.A. Rodriguez-Perez, Nanoporous PMMA: a novel system with different acoustic properties, Mater. Lett. 168 (2016) 76–79, https://doi.org/10.1016/j.matlet.2016.01.037.
[15] S. Costeux, Erratum: CO_2-blown nanocellular foams, J. Appl. Polym. Sci. 132 (2015) n/a, https://doi.org/10.1002/app.41887.
[16] D. Miller, P. Chatchaisucha, V. Kumar, Microcellular and nanocellular solid-state polyetherimide (PEI) foams using sub-critical carbon dioxide I. Processing and structure, Polymer 50 (2009) 5576–5584, https://doi.org/10.1016/j.polymer.2009.09.020.
[17] V. Kumar, J. Weller, Production of microcellular polycarbonate using carbon dioxide for bubble nucleation, J. Eng. Ind. 116 (1994) 413–420, https://doi.org/10.1115/1.2902122.
[18] V. Kumar, J.E. Weller, A model for the unfoamed skin on microcellular foams, Polym. Eng. Sci. 34 (1994) 169–173, https://doi.org/10.1002/pen.760340302.
[19] S.A. Shoyele, S. Cawthorne, Particle engineering techniques for inhaled biopharmaceuticals, Adv. Drug Deliv. Rev. 58 (2006) 1009–1029, https://doi.org/10.1016/j.addr.2006.07.010.
[20] P. Pavlínek, Transformation of the Czech automotive components industry through foreign direct investment, Eurasia Geogr. Econ. 44 (2008) 184–209, https://doi.org/10.2747/1538-7216.44.3.184.
[21] B.S.K. Gorle, I. Smirnova, W. Arlt, Adsorptive crystallization of benzoic acid in aerogels from supercritical solutions, J. Supercrit. Fluids 52 (2010) 249–257, https://doi.org/10.1016/J.SUPFLU.2010.01.006.
[22] T. Anukiruthika, P. Sethupathy, A. Wilson, K. Kashampur, J.A. Moses, C. Anandharamakrishnan, Multilayer packaging: advances in preparation techniques and emerging food applications, Compr. Rev. Food Sci. Food Saf. 19 (2020) 1156–1186, https://doi.org/10.1111/1541-4337.12556.
[23] S.G. Kazarian, M.F. Vincent, F.V. Bright, C.L. Liotta, C.A. Eckert, Specific intermolecular interaction of carbon dioxide with polymers, J. Am. Chem. Soc. 118 (1996) 1729–1736, https://doi.org/10.1021/ja950416q.
[24] O.S. Fleming, S.G. Kazarian, E. Bach, E. Schollmeyer, Confocal Raman study of poly (ethylene terephthalate) fibres dyed in supercritical carbon dioxide: dye diffusion and polymer morphology, Polymer 46 (2005) 2943–2949, https://doi.org/10.1016/j.polymer.2005.02.067.
[25] E. Aionicesei, M. Škerget, Ž. Knez, Measurement of CO_2 solubility and diffusivity in poly(l-lactide) and poly(d,l-lactide-co-glycolide) by magnetic suspension balance, J. Supercrit. Fluids 47 (2008) 296–301, https://doi.org/10.1016/j.supflu.2008.07.011.
[26] M.A. Fanovich, P. Jaeger, Sorption and diffusion of compressed carbon dioxide in polycaprolactone for the development of porous scaffolds, Mater. Sci. Eng. C 32 (2012) 961–968, https://doi.org/10.1016/j.msec.2012.02.021.
[27] R. Satija, D.L. Jacobson, M. Arif, S.A. Werner, In situ neutron imaging technique for evaluation of water management systems in operating PEM fuel cells, J. Power Sources 129 (2004) 238–245, https://doi.org/10.1016/j.jpowsour.2003.11.068.
[28] C.M. Roland, Neutron Scattering in the Analysis of PolymersUpdate based on the original article by D. G. Bucknall, Encyclopedia of Analytical Chemistry, © 2000, in: D.G. Bucknall (Ed.), Encyclopedia of Analytical Chemistry, John Wiley & Sons, Ltd., 2012, pp. 1–27, https://doi.org/10.1002/9780470027318.a2022.pub2.
[29] M.M.R. Williams, The mathematics of diffusion, Ann. Nucl. Energy 4 (1977) 205–206, https://doi.org/10.1016/0306-4549(77)90072-X.
[30] X. Han, K.W. Koelling, D.L. Tomasko, L.J. Lee, Continuous microcellular polystyrene foam extrusion with supercritical CO_2, Polym. Eng. Sci. 42 (2002) 2094–2106, https://doi.org/10.1002/pen.11100.
[31] M. Tang, T.-B. Du, Y.-P. Chen, Sorption and diffusion of supercritical carbon dioxide in polycarbonate, J. Supercrit. Fluids 28 (2004) 207–218, https://doi.org/10.1016/S0896-8446(03)00045-7.
[32] Y. Sato, M. Yurugi, K. Fujiwara, S. Takishima, H. Masuoka, Solubilities of carbon dioxide and nitrogen in polystyrene under high temperature and pressure, Fluid Phase Equilib. 125 (1996) 129–138, https://doi.org/10.1016/S0378-3812(96)03094-4.
[33] R.G. Wissinger, M.E. Paulaitis, Swelling and sorption in polymer–CO_2 mixtures at elevated pressures, J. Polym. Sci. Part B Polym. Phys. 25 (1987) 2497–2510, https://doi.org/10.1002/polb.1987.090251206.
[34] D.L. Tomasko, H.B. Li, D.H. Liu, X.M. Han, M.J. Wingert, L.J. Lee, K.W. Koelling, A review of CO(2) applications in the processing of polymers, Ind. Eng. Chem. Res. 42 (2003) 6431–6456, https://doi.org/Doi 10.1021/Ie030199z.
[35] D.A. Bostain, J.S. Brenizer, P.M. Norris, Neutron radioscopic measurement of water adsorption coefficients in aerogels, Res. Nondestruct. Eval. 14 (2002) 47–57, https://doi.org/10.1080/09349840209409703.
[36] S1875389217300883, (n.d.).
[37] P. Vontobel, E.H. Lehmann, R. Hassanein, G. Frei, Neutron tomography: method and applications, Phys. B Condens. Matter 385–386 I (2006) 475–480, https://doi.org/10.1016/j.physb.2006.05.252.
[38] Y.B. Melnichenko, G.D. Wignall, D.R. Cole, H. Frielinghaus, Adsorption of supercritical CO2 in aerogels as studied by small-angle neutron scattering and neutron transmission techniques, J. Chem. Phys. 124 (2006) 1–11, https://doi.org/10.1063/1.2202324.
[39] N. Kardjilov, A. Hilger, I. Manke, J. Banhart, CONRAD-2: the neutron imaging instrument at HZB, Neutron News 25 (2014) 23–26, https://doi.org/10.1080/10448632.2014.902700.
[40] N. Kardjilov, A. Hilger, I. Manke, R. Woracek, J. Banhart, CONRAD-2: the new neutron imaging instrument at the Helmholtz-Zentrum Berlin, J. Appl. Crystallogr. 49 (2016) 195–202, https://doi.org/10.1107/S1600576715023353.
[41] H. Guo, V. Kumar, Solid-state poly(methyl methacrylate) (PMMA) nanofoams. Part I: low-temperature CO_2 sorption, diffusion, and the depression in PMMA glass transition, Polymer 57 (2015) 157–163, https://doi.org/10.1016/j.polymer.2014.12.029.
[42] J. Vlassenbroeck, B. Masschaele, V. Cnudde, M. Dierick, K. Pieters, L. Van Hoorebeke, P. Jacobs, Octopus 8: a high performance tomographic reconstruction package for x-ray tube and synchrotron micro-CT, Adv. X-Ray Tomogr. Geomater. (2010) 167–173, https://doi.org/10.1002/9780470612187.ch13.
[43] M. Alshipli, N.A. Kabir, R. Hashim, M.W. Marashdeh, A.A. Tajuddin, Measurement of attenuation coefficients and CT numbers of epoxy resin and epoxy-based Rhizophora spp particleboards in computed tomography energy range, Radiat. Phys. Chem. 149 (2018) 41–48, https://doi.org/10.1016/j.radphyschem.2018.04.001.
[44] J. Vlassenbroeck, M. Dierick, B. Masschaele, V. Cnudde, L. Van Hoorebeke, P. Jacobs, Software tools for quantification of X-ray microtomography at the UGCT, Nucl. Instrum. Methods Phys. Res. Sect. A Accel. Spectrom. Detect. Assoc. Equip. 580 (2007) 442–445, https://doi.org/10.1016/j.nima.2007.05.073.
[45] C. Forest, P. Chaumont, P. Cassagnau, B. Swoboda, P. Sonntag, CO_2 nano-foaming of nanostructured PMMA, Polymer 58 (2015) 76–87, https://doi.org/10.1016/j.polymer.2014.12.048.
[46] L. Nikitin, E. Said-Galiyev, R.A. Vinokur, A.R. Khokhlov, Poly (methyl methacrylate) and Poly (butyl methacrylate) swelling in supercritical carbon dioxide, Macromolecules 35 (2002) 934–940, https://doi.org/10.1021/ma010271.
[47] A. Rajendran, B. Bonavoglia, N. Forrer, G. Storti, M. Mazzotti, M. Morbidelli, Simultaneous measurement of swelling and sorption in a supercritical CO2-poly (methyl methacrylate) system, Work (2005) 2549–2560.
[48] B. Bonavoglia, G. Storti, M. Morbidelli, Modelling of the Sorption and Swelling Behavior of Semi-crystalline Polymers in Supercritical CO2, October. (2005) 41–44.
[49] H. Guo, A. Nicolae, V. Kumar, Solid-state poly(methyl methacrylate) (PMMA) nanofoams. Part II: low-temperature solid-state process space using CO_2 and the resulting morphologies, Polymer 70 (2015) 231–241, https://doi.org/10.1016/j.polymer.2015.06.031.
[50] Y. Sato, K. Fujiwara, T. Takikawa, Sumarno, S. Takishima, H. Masuoka, Solubilities and diffusion coefficients of carbon dioxide and nitrogen in polypropylene, high-density polyethylene, and polystyrene under high pressures and temperatures, Fluid Phase Equilib. 162 (1999) 261–276, https://doi.org/10.1016/S0378-3812(99)00217-4.
[51] S. Doroudiani, C.E. Chaffey, M.T. Kortschot, Sorption and diffusion of carbon dioxide in wood-fiber/polystyrene composites, J. Polym. Sci. Part B Polym. Phys. 40 (2002) 723–735, https://doi.org/10.1002/polb.10129.
[52] H. Guo, V. Kumar, Some thermodynamic and kinetic low-temperature properties of the PC-CO_2 system and morphological characteristics of solid-state PC nanofoams produced with liquid CO_2, Polymer 56 (2015) 46–56, https://doi.org/10.1016/j.polymer.2014.09.061.
[53] K.F. Webb, A.S. Teja, Solubility and diffusion of carbon dioxide in polymers, Fluid Phase Equilib. 158–160 (1999) 1029–1034, https://doi.org/10.1016/S0378-3812(99)00153-3.
[54] M. Pantoula, C. Panayiotou, Sorption and swelling in glassy polymer/carbon dioxide systems, J. Supercrit. Fluids 37 (2006) 254–262, https://doi.org/10.1016/j.supflu.2005.11.001.
[55] S. Enders, H. Kahl, J. Winkelmann, Interfacial properties of polystyrene in contact with carbon dioxide, Fluid Phase Equilib. 228–229 (2005) 511–522, https://doi.org/10.1016/j.fluid.2004.10.001.
[56] J. Crank, The Mathematics of Diffusion, Oxford University Press, 1975, https://doi.org/10.1016/0306-4549(77)90072-X.